Cationic Polymerization in Rotating Packed Bed Reactor: Experimental and Modeling

Jian-Feng Chen, Hua Gao, Hai-Kui Zou, Guang-Wen Chu, Lei Zhang, Lei Shao, and Yang Xiang
Key Lab for Nanomaterials, Ministry of Education, Research Center of Ministry of Education for High Gravity Engineering and Technology, Beijing University of Chemical Technology, Beijing 100029, P.R. China

Yi-Xian Wu
State Key Lab of Chemical Resource Engineering, Beijing University of Chemical Technology, Beijing 100029, P.R. China

DOI 10.1002/aic.11911
Published online December 30, 2009 in Wiley InterScience (www.interscience.wiley.com).

On the basis of analysis of key engineering factors predominating in cationic polymerization, butyl rubber (IIR) as an example was synthesized by cationic polymerization in the high-gravity environment generated by a rotating packed bed (RPB) reactor. The influence of the rotating speed, packing thickness, and polymerization temperature on the number average molecular weight (M_n) of IIR was studied. The optimum experimental conditions were determined as rotating speed of 1200 r min^{-1}, packing thickness of 40 mm and polymerization temperature of 173 K, where IIR with M_n of 289,000 and unimodal molecular weight distribution of 1.99 was obtained. According to the experimental results and elementary reactions, a model for the prediction of M_n was developed, and the validity of the model was confirmed by the fact that most of the predicted M_ns agreed well with the experimental data with a deviation within 10%. © 2009 American Institute of Chemical Engineers *AIChE J,* 56: 1053–1062, 2010
Keywords: cationic polymerization, butyl rubber, rotating packed bed, modeling, number average molecular weight

Introduction

The past decade has seen a rapid development and wide application of cationic polymerization for the synthesis of a wide variety of novel materials with potential commercial interest, such as polyisobutylene, polybutenes, butyl rubber (IIR), etc.[1–12]

The rate constants of propagation (k_p) in the cationic polymerization vary considerably, e.g., k_p's from 10^3 to 10^9 L mol^{-1} s^{-1} have been reported for isobutylene polymerization.[13,14] It is proposed that the discrepancy in k_p reported for various cationic polymerizations is due to different mechanistic interpretations and assumptions.[15] Two general methods, diffusion clock (DC) and ionic species concentration methods, are typically used to determine the propagation rate constants in cationic polymerization of vinyl monomers. Both of the methods give similar values of k_p ($k_p = 10^4$–10^5 L mol^{-1} s^{-1}) for the polymerization of some substituted styrenes, while considerable higher values of k_p ($k_p = 10^9$ L mol^{-1} s^{-1}) are obtained by DC method in the case of styrene and isobutylene.[16–18] Despite large variation with some monomers, it is generally accepted that the rate constants of propagation in the cationic polymerization of alkenes are similar for most systems with $k_p = 10^{5 \pm 1}$ L mol^{-1} s^{-1}.[16,19] Therefore, the cationic polymerization features an extremely rapid intrinsic reaction rate with apparent reaction rate affected significantly by micromixing.[20–24]

Micromixing is the final stage of turbulent mixing and consists of the viscous-convective deformation of fluid elements, followed by molecular diffusion. It is believed that micromixing plays a very important role in chemical industry when the time scale of the chemical reaction involved is

Correspondence concerning this article should be addressed to J.-F. Chen at chenjf@mail.buct.edu.cn and Y.-X. Wu at yxwu@263.net.

at the same magnitude as or smaller than the time scale of the mixing process. Industrial processes, such as crystallization, precipitation and polymerization, are greatly influenced by micromixing. In these extremely rapid processes, the reactions may occur or complete before the reactants accomplish homogeneous mixing at the molecule scale. Consequently, the qualities of the product such as particle size distribution, molecular weight and its distribution are significantly influenced by micromixing.[25,26]

Conventional cationic polymerization reactors include stirred tank reactor,[27] continuous flow stirred reactor,[28,29] etc. These reactors usually lead to poor mixing, broad residence time distribution and long residence time,[23,24,30] resulting in the difficulty to control the number average molecular weight (M_n) and molecular weight distribution (MWD).[12,23,31] Therefore, a novel reactor with good micromixing performance is a long sought-after goal in cationic polymerization and of significant importance to further improving the production efficiency and product quality.

Analysis of polymerization and selection of reactor type

Cationic polymerization process is characterized by initiation, propagation, termination and chain transfer. The propagation reaction is first order with respect to monomer concentration, so the reactive characteristic time $t_{1/2}$ is:

$$t_{1/2} = \frac{\ln 2}{k_p} \tag{1}$$

The value of propagation rate constant for isobutylene cationic polymerization about $10^{5 \pm 1}$ L mol^{-1} s^{-1} could be chosen for estimation based on the reported data.[16,19] Because of the copolymerization of isobutylene with lower reactive monomer isoprene (1.5–2.0%), the propagation rate constant with lower values of 10^4–10^5 L mol^{-1} s^{-1} could be adopted. Therefore $t_{1/2}$ is estimated at about 0.01–0.1 ms.

Micromixing, which determines the local spatial distribution of the monomers, is very critical in the scale-up of the cationic polymerization process. Micromixing has no influence on the apparent propagation reaction rate in the region of $t_m \leq t_{1/2}$ and has significant influence on the apparent propagation reaction rate when $t_m > t_{1/2}$, where, t_m is the micromixing characteristic time for species reaching a maximum mixed state at the molecule level. Because of the very strong nonlinearity of propagation, micromixing should be intensified to reach the region of $t_m \leq t_{1/2}$, so that the propagation rates at different locations will be nearly the same, and M_n and MWD can be controlled at a desired value and a uniform level.

The characteristic time of micromixing was estimated by Li et al. as,[32]

$$t_m = k_m(v/\varepsilon)^{1/2} \tag{2}$$

where k_m is a constant, $k_m = 16$, as presented by Chen et al.[33] In a typical stirred tank, t_m is estimated to be in the region of 5–50 ms.[33] Therefore, $t_m > t_{1/2}$, which implies that M_n and MWD in a stirred tank cannot be easily controlled for the extremely rapid cationic polymerization and the scale-up effect will play a more important role owing to the poor micromixing.

Rotating Packed Bed (RPB) is an apparatus consisting mainly of a packed rotator and a fixed casing. The basic principle of RPB is to create a high-gravity environment via the action of centrifugal force as so called "Higee".[34,35] The fluids going through the packing of RPB are spread or split into very fine droplets, threads, and thin films by the strong shear, resulting in a significant intensification of micromixing and mass transfer between the fluid elements. The rate of mass transfer between gas and liquid in RPB is 1–3 orders of magnitude larger than that in a conventional packed bed, allowing a dramatic reduction of reaction time.[33,36–40] In terms of these unique features, RPB has been successfully applied to the preparation of nanoparticles and is regarded as a promising industrial platform for the production of inorganic nanopowders.[38,40]

The value of t_m in RPB is estimated to be 0.01–0.1 ms,[25] which could meet the requirement of $t_m \leq t_{1/2}$ and therefore M_n and MWD could be well controlled when RPB is employed for polymer synthesis reactions limited by micromixing. It can be thus deduced that RPB is a promising reactor for cationic polymerization.

IIR is a copolymer of isobutylene and isoprene and generally contains 1.5–2.0% of isoprene units. Because of low gas permeability, good thermal and oxidative stability, and excellent chemical resistance, IIR is one of the most useful rubbers in a wide variety of applications, including tires, inner tubes, tire inner liners, and rubber tire-curing bladders.[41–45] IIR synthesis via the cationic copolymerization of isobutylene with a small amount of isoprene in RPB was carried out for the first time in this study. It was found that high-quality IIR was synthesized in RPB reactor due to the significant intensification of micromixing. Furthermore, a theoretical model for the prediction of M_n was also developed and validated by experimental results.

Experimental Section

Reagents

Isobutylene (polymer grade, purity > 99%, Beijing Yanshan Petrochemical Group), isoprene (polymer grade, purity > 99%, Beijing Yanshan Petrochemical Group) and aluminum trichloride ($AlCl_3$, purity > 99%, Belgium Acros Organic Chemical) were used as received. Dichloromethane (CH_2Cl_2, purity > 99.5%, Beijing Yili Fine Chemical) was dried prior to use by distillation from calcium hydride

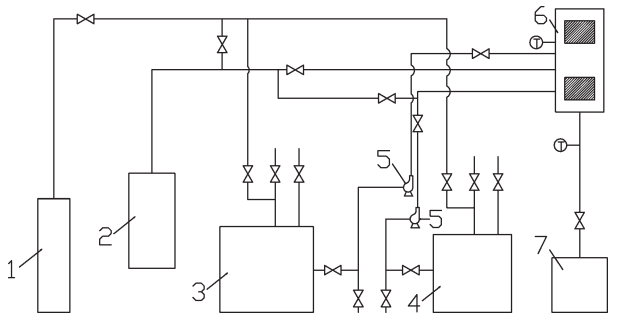

Figure 1. Schematic diagram of IIR synthesis set-up.

(1) nitrogen cylinder, (2) coolant tank, (3) isobutylene, isoprene and dichloromethane tank, (4) aluminum trichloride and dichloromethane tank, (5) metering pump, (6) RPB, (7) IIR tank.

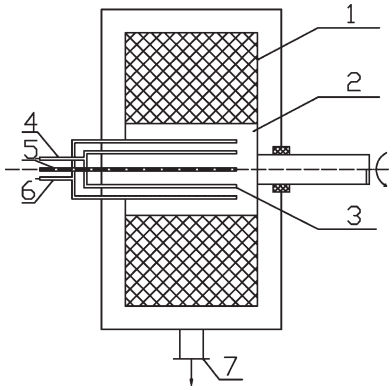

Figure 2. Schematic diagram of RPB for IIR synthesis.

(1) packing, (2) rotator, (3) liquid distributor, (4) monomer inlet, (5) catalyst inlet, (6) coolant inlet, (7) IIR outlet.

(CaH_2, purity > 99.5%, Tianjin Jinke Fine Chemical Institute). Liquid nitrogen (purity > 99.99995%, Beijing Ruyuan Ruquan Science and Technology) was employed as the coolant.

Instrumentation

Gel Permeation Chromatography (GPC, 515–2410, Waters) was employed to determine the M_n of IIR products. Tetrahydrofuran (THF) served as the solvent of IIR with 20 mg of IIR dissolved in 10 ml of THF and the mobile phase flowed at 1.0 ml/min.

Experimental procedures

The experimental set-up for IIR synthesis is shown schematically in Figure 1. The RPB for IIR synthesis consists mainly of a packed rotator, a fixed casing, and different liquid inlets to introduce the monomers, catalyst, and coolant, respectively (Figure 2). The inner and outer diameters of the rotator are 150 mm and 258 mm, respectively, and the axial length of the rotator is 50 mm. The rotator is installed inside the fixed casing and rotates at the speed of several hundreds and thousands rpm.

All the pipelines and equipment were swept by nitrogen before use in order to remove the moisture and air. Isobutylene, isoprene, and dichloromethane were added into tank (3) to form a monomers solution of 9 L with [isobutylene] = 2.7 mol L^{-1} and [isoprene] = 0.05 mol L^{-1}, and 900 mL of the catalyst solution of aluminum trichloride and dichloromethane ($[AlCl_3] = 1.1 \times 10^{-2}$ mol L^{-1}) was added into tank (4). The

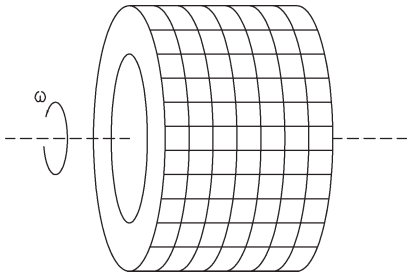

Figure 3. Sketch of a wire-mesh packing.

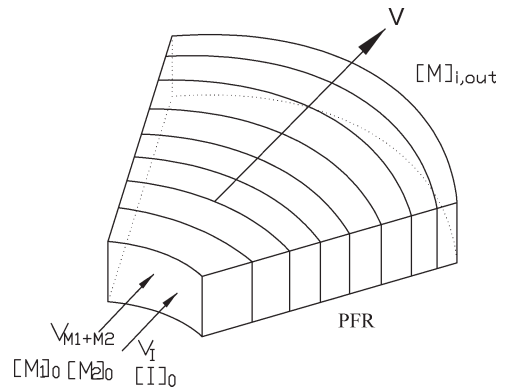

Figure 4. Diagram of liquid flow in the packing.

pipelines and RPB reactor were prechilled to the set temperature by the coolant. When the temperature of reactants in tanks (3) and (4) reached the polymerization temperature, the reactants were pumped into RPB at a volumetric flow rate ratio of monomers/catalyst = 10 to conduct the polymerization reaction. Theas- synthesized IIR product was collected by tank (7). When the system reached a steady state, the IIR slurry sample was taken and treated for M_n and MWD analyses. The M_n of IIR at different radial positions of the packing was obtained by changing the packing thickness.

Model Development

Modeling of IIR synthesis in RPB reactor

The packing of RPB was assumed to be composed of a number of concentric cages as shown in Figure 3. Under the action of centrifugal force, liquid sprayed on the inner edge of the packing moves outwards throughout the void space of the packing, and finally flows out of the outer edge of the packing. It was also assumed that the liquid had the same residence time in the packing and the liquid flow pattern at radial direction was plug flow (Figure 4), and the liquid phase existed as dispersed droplets in the packing based on previous visual observations of liquid flow in RPB.[33,46,47] The exchange of reactants among droplets on every cage was described by a coalescence-redispersion model,[48] which

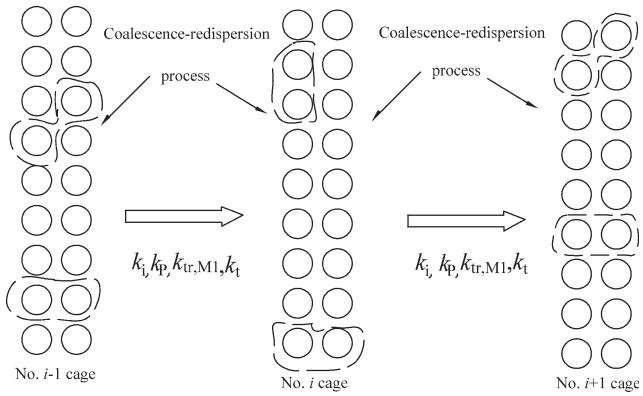

Figure 5. Illustration of coalescence-redispersion of droplets on cages and polymerization between two adjacent cages.

Initiation: $I + LA \rightleftharpoons I^+LA^-$

$$I^+LA^- + M_1 \xrightarrow{k_i} P_1^+LA^-$$

$$\text{Rate: } r_i = k_i[I][M_1] \quad (4)$$

Propagation: $P_n^+LA^- + M_1 \xrightarrow{k_{p,M_1}} P_{1(n+1)}^+LA^-$

$$\text{Rate: } r_{p,M1} = k_{p,M_1}[A][M_1] \quad (5)$$

$$P_n^+LA^- + M_2 \xrightarrow{k_{P,M_2}} P_{2(n+1)}^+LA^-$$

$$\text{Rate: } r_{p,M_2} = k_{p,M_2}[A][M_2] \quad (6)$$

Chain Transfer to the monomer: $P_n^+LA^- + M_1 \xrightarrow{k_{tr,M1}} P_{n1} + P_1^+LA^-$

$$\text{Rate: } r_{tr,M_1} = k_{tr,M_1}[A][M_1] \quad (7)$$

Termination: $P_n^+LA^- \xrightarrow{k_t} P_{n2} + LA$

$$\text{Rate: } r_t = k_t[A] \quad (8)$$

Scheme 1. Simplified mechanism for IIR synthesis via cationic polymerization.

treated the liquid as numerous miscible droplets and mixing was realized by collision, coalescence, and redispersion of two droplets, as illustrated in Figure 5. In the coalescence-redispersion model, all droplets have the same size and the coalescence of any two droplets is followed instantaneously by redispersion into two identical droplets with uniform concentration, and the participated droplets on each cage are chosen by Monte Carlo stochastic function method.

When the coalescence–redispersion model was used to predict the effects of micromixing during liquid-liquid reactive precipitation in RPB, the concentration of each component was assumed to be homogeneous in every active droplet. The model was used to establish polymerization kinetics equations of active droplets.

Estimation of Parameters

Droplet diameter and number. The mean diameter of droplets in RPB was reported to be 0.1–0.3 mm.[46] On the basis of the mean diameter of the droplets and the liquid flow rate, the total number of droplets was calculated as 550, which was thus used as the initial droplet number in the following calculation.

Residence time. The mean residence time of liquid throughout the packing in RPB under different experimental conditions was reported by Guo.[39,49] The residence time of droplets between two adjacent packing cages was determined as,

$$t_i = \frac{\tau}{N_L} \quad (3)$$

Modeling of the polymerization kinetics

This study employed a "chain analysis" method to develop the model.[50–54] In chain analysis method macromolecules with various chain lengths and compositions can be regarded as composed of different structural units. For one given polymer, the variety of structural units is limited to a certain number, so complex macromolecules can be analyzed through these definite structural units.[51,52]

The kinetic scheme adopted for the synthesis of IIR by cationic polymerization involves initiation, propagation, chain transfer to the monomer, and termination as shown in Scheme 1.[15,22,24,51,52]

Several denotations are defined as follows.

M_1 and M_2 represent isobutylene and isoprene monomers respectively:

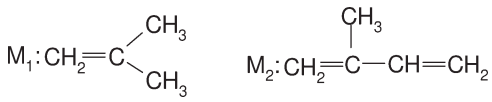

C_1 and C_2 represent two structural units of IIR respectively:

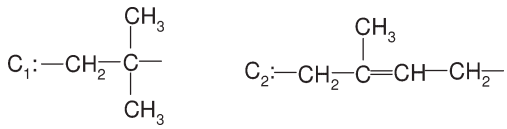

A represents the growing chain unit:

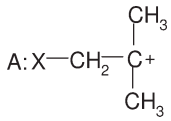

E_1 represents the end group of IIR:

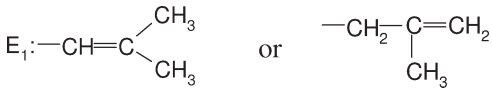

E_2 represents the end group of IIR:

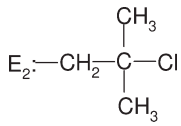

I represents the initiator, P_1, P_n^+ represents A, $P_{1(n+1)}$ represents AC_1, $P_{2(n+2)}$ represents AC_2, P_{n1} respresents PE_1, P_{n2} respresents PE_2, P represents dead polymer.

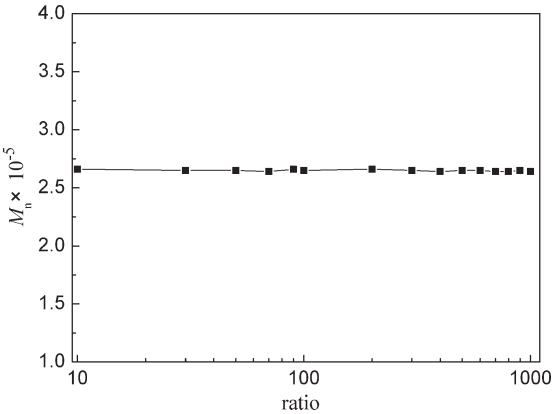

Figure 6. The ratio of k_p(IB)/k_p(IP) vs. M_n.

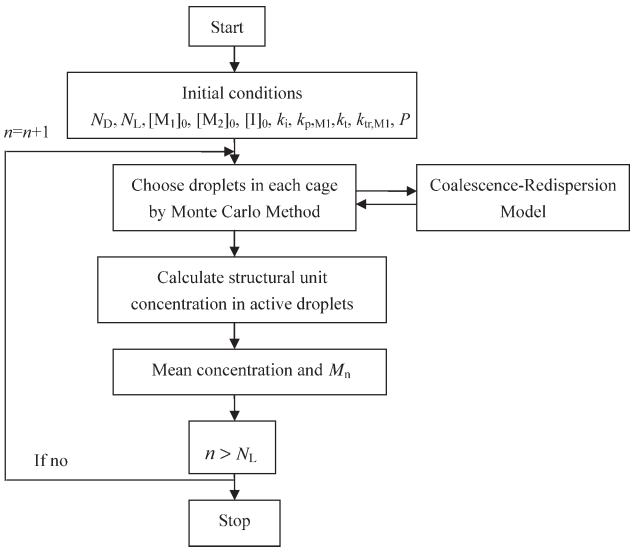

Figure 7. Simulation flow chart for the model.

In the process of polymerization, IIR with different components and chain lengths is composed of structural units with varied amounts of C_1, C_2, E_1, E_2, and A. Therefore, the determination of M_n can be converted into the calculation of the five units of C_1, C_2, E_1, E_2, and A.

As shown in Scheme 1, cationic polymerization involves several distinct kinetic steps. The polymerization starts with the formation of a growing chain unit (A), and the chain propagation proceeds linearly, incorporating M_1 and M_2 groups along the polymer backbone.

The following assumptions were employed in dealing with the reaction kinetics:

(1) Equal activity assumption: The activity of macromolecules with different chain length was assumed to be the same.[31,53]

(2) Linear chain propagation assumption: Linear chain propagation assumption is also named long chain approximation, where macromolecule is regarded as a linear long chain without branches. This assumption can simplify the modeling derivation without sacrificing the validity of the model in predicting the polymerization kinetics.[31,54]

(3) As $k_p(IB) > k_p(IP)$, it was assumed that $k_{p,M_1} = 10 \times k_{p,M_2}$ in our calculation. Moreover, it is shown in Figure 6 that the $k_p(IB)/k_p(IP)$ ratio does not influence the simulated M_n.

The generation/consumption rates of every reaction can be written in the following forms:

$$\frac{d[M_1]}{dt} = -r_i - r_{p,M_1} - r_{tr,M_1} = -k_i[I][M_1] - k_{p,M_1}[A][M_1] - k_{tr,M_1}[A][M_1] \quad (9)$$

$$\frac{d[M_2]}{dt} = -r_{p,M_2} = -k_{p,M_2}[A][M_2] \quad (10)$$

$$\frac{d[A]}{dt} = r_i - r_t = k_i[I][M_1] - k_t[A] \quad (11)$$

$$\frac{d[I]}{dt} = -r_i = -k_i[I][M_1] \quad (12)$$

$$\frac{d[E_1]}{dt} = r_{tr,M_1} = k_{tr,M_1}[A][M_1] \quad (13)$$

$$\frac{d[C_1]}{dt} = r_{p,M_1} = k_{p,M_1}[A][M_1] \quad (14)$$

$$\frac{d[C_2]}{dt} = r_{p,M_2} = k_{p,M_2}[A][M_2] \quad (15)$$

$$\frac{d[E_2]}{dt} = r_t = k_t[A] \quad (16)$$

The reaction rate constants in the above equations were experimentally determined and applied to the derivation of the polymerization kinetic model of IIR.

Calculation of M_n

The concentration of structural units in the reactor at different time can be calculated from the reaction kinetics. M_n can be calculated from the number-average molecule weight definition and the linear chain assumption of chain analysis.[31,53,54] According to the proposed mechanism, the theoretical M_n was predicted by the following equation,

$$M_n = \frac{W}{n} = \frac{\sum_i n_i M_i}{\sum_i n_i} = 2 \times \frac{\sum_i ([C_i] \times M_{w_{C_i}}) + \sum_i ([E_i] \times M_{w_{E_i}}) + [A] \times M_{w_A}}{[A] + \sum_i [E_i]} \quad (17)$$

Via Eqs. 9–17, the concentration of every structural unit on each active droplet was obtained, and the average concentration of every structural unit for all droplets in No. i cage ($\overline{[C_{i,k}]}$) was calculated as,

$$\overline{[C_{i,k}]} = \frac{\sum_{g=1}^{N_D} [C_{i,k,g}]}{N_D} \quad (18)$$

Then the M_n at No. i cage was calculated by the mean concentration of every structural unit.

Numerical solution

The proposed differential Eqs. 9–18 need to be solved by taking into account the boundary conditions to simulate the M_n of IIR synthesized in RPB. The concentrations of the monomers and catalyst entering the RPB at its inner edge were known. In the process of computation, Monte Carlo random functions were adopted to characterize the coalescence–redispersion of liquid through the packing.

Table 1. Parameter Values Used in the Model

N_D	N_L	δ, mm	r_i, mm
550	60	0.9	75

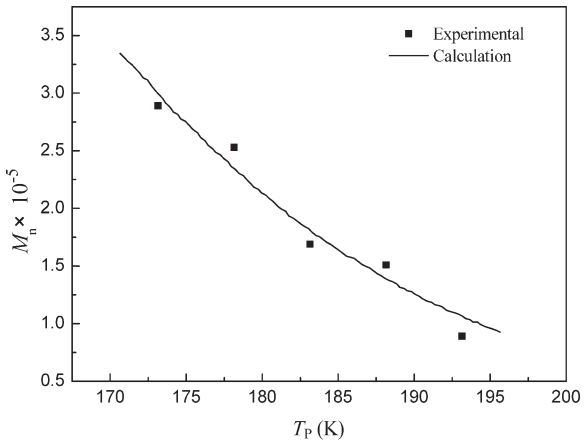

Figure 8. Experimental and calculated M_n vs. T_p (N = 1200 r min^{-1}, D = 40 mm).

Concentration of every structural unit on each cage was solved through the Runge–Kutta numerical method.[52,55] A MATLAB program was used to solve the model equations. Figure 7 illustrates the simulation flow chart for the model. All differential equations involved were integrated by Runge–Kutta method. The specific set of relevant parameters used in the model is given in Table 1.

Results and Discussion

A series of experiments were carried out through changing operation conditions such as rotating speed (N), packing thickness (D), and polymerization temperature (T_p). In the experiments, the initial conditions were $[M_1]_0 = 2.7$ mol L^{-1}, $[M_2]_0 = 0.05$ mol L^{-1}, $[I]_0 = 0.011$ mol L^{-1}, and the flow rate ratio of the monomers to the catalyst was 10:1.

Polymerization kinetics parameters were calculated based on the data of the polymerization temperature experiment while the coalescence probability was determined by the data of the rotating speed experiment. The validity of the model was demonstrated by a comparison with the data of the packing thickness experiment.

Estimation of polymerization kinetics parameters

Effect of T_p. Figure 8 gives the calculated and experimental M_n as a function of T_p. It can be seen that the M_n of IIR decreased as T_p increased. The effects of the temperature on the rate constants can be explained from the activation energy of the reactions. The total activation energy of IIR synthesis reaction is negative,[56] so the reaction rate increases with decreasing T_p. At the same time, decreasing T_p is favorable for the formation of active centers. The energy of chain termination is much higher than that of chain propagation, so the decrease of T_p is beneficial to chain propagation.[24] Therefore, to obtain IIR with high molecular weight, it is essential to carry out the polymerization at low temperature, where the rate of chain-transfer reaction is reduced, leading to the increase in M_n.[23,24] The M_n of IIR synthesized at 173 K reached 289,000 and polydispersity of the IIR was 1.99, exhibiting a unimodal molecular weight distribution. It can also be seen from Figure 8 that the calculated M_ns fit well with the experimental M_ns.

Figure 9 illustrates calculation process of the polymerization kinetics parameter k_{p,M_1} based on the temperature experiment data.

Estimation of k_{p,M_1}.

Figure 10a shows the effect of k_{p,M_1} on M_n. Simulation by the model indicated that M_n increased as k_{p,M_1} increased from 1×10^3 to 1×10^{10} L mol^{-1} s^{-1}, and M_n increased sharply when k_{p,M_1} was larger than 1×10^8 L mol^{-1} s^{-1}, with M_n reaching 14.4×10^5 when k_{p,M_1} was 1×10^9 L mol^{-1} s^{-1}. It is also deduced from Figures 8 and 10a that the decrease of temperature resulted in the increase of k_{p,M_1}, leading to the increase of M_n.

Table 2 gives the data of M_n, T_p and k_{p,M_1}. M_n and T_p were obtained from the experiments and k_{p,M_1} was calculated by the model. It can be seen from Table 2 that with the experimental M_n at about 1×10^5–3×10^5, k_{p,M_1} was in the range of 10^4–10^5 L mol^{-1} s^{-1} in this study. Propagation rate constant for cationic polymerization of alkenes is generally accepted at about $10^{5 \pm 1}$ L mol^{-1} s^{-1}.[16,19] It was also reported that propagation rate constant for cationic polymerization of isobutylene ($k_{p,IB}$) is $k_{p,IB} = 9.1 \times 10^3$ L mol^{-1} s^{-1} (Ionizing radiation, CH_2Cl_2, 195 K)[21,22] and $k_{p,IB} = 7.9 \times 10^5$ L mol^{-1} s^{-1} (Light/VCl_4, in bulk, 253 K).[22] Therefore, it can be seen that our proposed k_{p,M_1} is in the same magnitude order range as reported in the literature.

The apparent activation energy (E_a) was calculated as -23.8 kJ mol^{-1} from the slope of Arrhenius plot of $\ln k_{p,M_1}$ vs. $1/T_p$, which is somewhat higher than that reported by Faust et al. (-34 kJ mol^{-1}),[14] Storey et al. (-30.1 kJ mol^{-1}),[56] and Puskas et al. (-26.4 kJ mol^{-1}).[57]

Estimation of k_i.

It can be assumed $k_i \approx k_p$,[15] so k_i was chosen as 1×10^4 L mol^{-1} s^{-1} in this study.

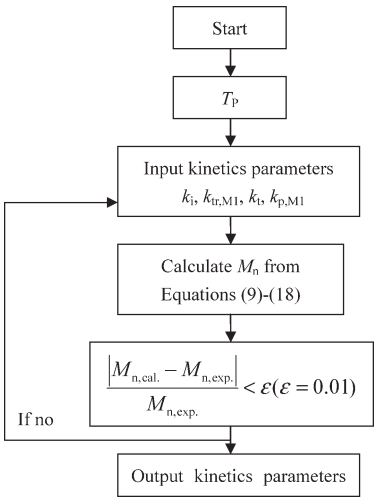

Figure 9. Flow chart of kinetics parameters calculation.

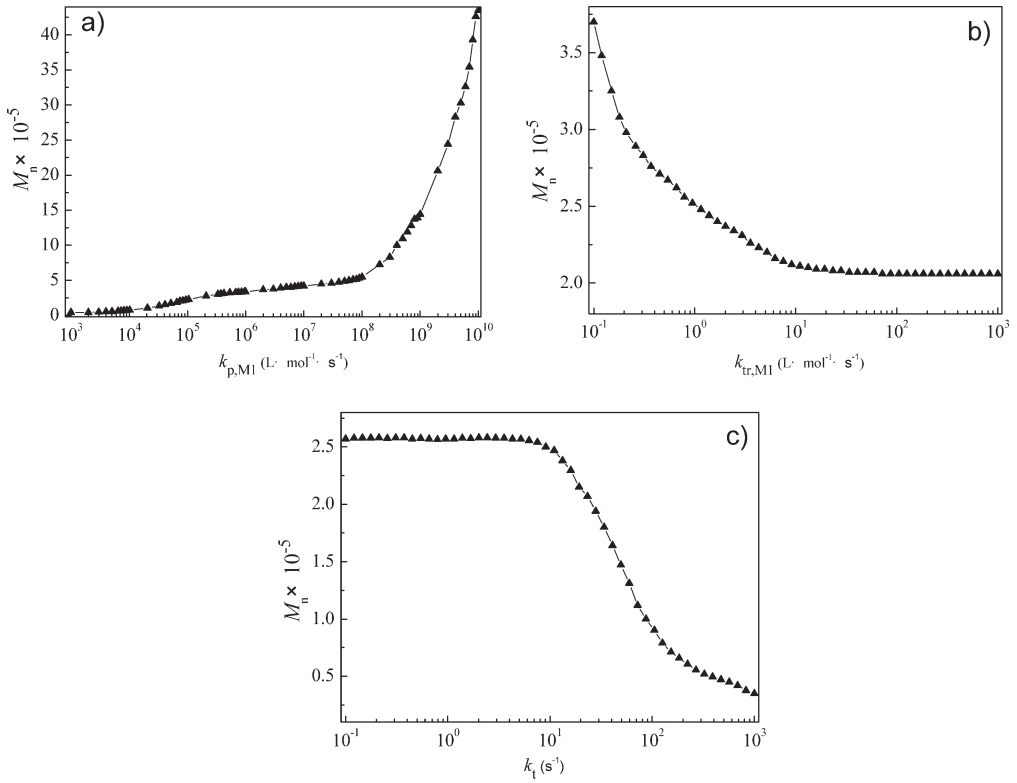

Figure 10. Effect of polymerization kinetics parameters on M_n: (a) k_{p,M_1}, (b) $k_{tr,M1}$, (c) k_t.

Estimation of k_{tr,M_1}.

Figure 10b shows the effect of $k_{tr,M1}$ on M_n. It can be seen that M_n decreased as $k_{tr,M1}$ increased from 1×10^{-1} to 1×10^3 L mol^{-1} s^{-1}. When $K_{tr,M1} \geq 10$ L mol^{-1} s^{-1}, M_n almost reached a fixed value, and the effect of k_{tr,M_1} on M_n can be neglected, so k_{tr,M_1} was chosen as 10 L mol^{-1} s^{-1}.

It was calculated that $k_{tr,M1}/k_p \approx 10^{-4}$ in this study, which is in the same magnitude order range as reported in the literature.[58]

Estimation of k_t.

Figure 10c shows the effect of k_t on M_n. It can be seen that M_n decreased as k_t increased from 1×10^{-1} to 1×10^3 s^{-1}. When $k_t \leq 10$ s^{-1}, M_n almost reached a fixed value, and the effect of k_t on M_n can be neglected, so k_t was chosen as 10 s^{-1}.

*Estimation of coalescence probability (*P*)*

Effect of N. Figure 11 presents the calculated and experimental data of the influence of N on the M_n of IIR. The experimental results demonstrate that M_n increased sharply with an increase in the N of RPB ranging from 600 to 1200 r min^{-1} and then leveled off when N was more than 1200 r min^{-1}. The optimum rotating speed was thus determined as 1200 r min^{-1} where IIR with M_n = 289,000 and MWD = 1.99 was obtained. It can also be seen from Figure 11 that the calculated M_ns fit well with the experimental M_ns.

The reasons that M_n increases with an increasing N under certain conditions may be explained as follows. Vigorous impingement between liquid and the packing is achieved with an increase in N, and the increase in collision probability among the liquid elements results in better mixing effects. In addition, there is also an increase in both the

Table 2. The Relationship of T_p and k_{p,M_1} (N = 1200 r min^{-1}, D = 40 mm)

$M_n \times 10^{-5}$	T_p (K)	$k_{p,M_1} \times 10^{-4}$	$(1/T_p) \times 10^3$ (1/K)	ln k_{p,M_1}
0.89	193	2.67	5.18	10.19
1.50	188	3.15	5.32	10.36
1.67	183	4.87	5.46	10.79
2.53	178	10.2	5.62	11.53
2.89	173	12.68	5.78	11.75

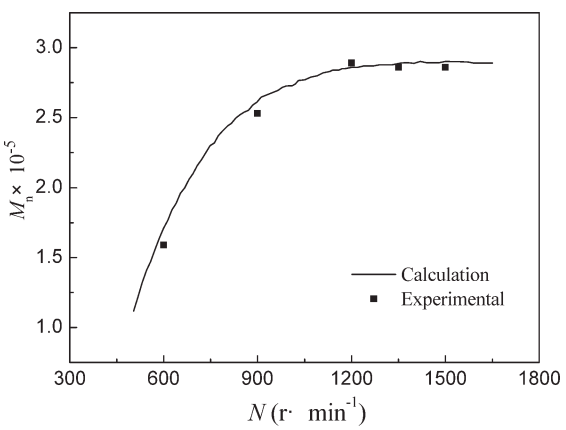

Figure 11. Experimental and calculated M_n vs. N (T_p = 173 K, D = 40 mm).

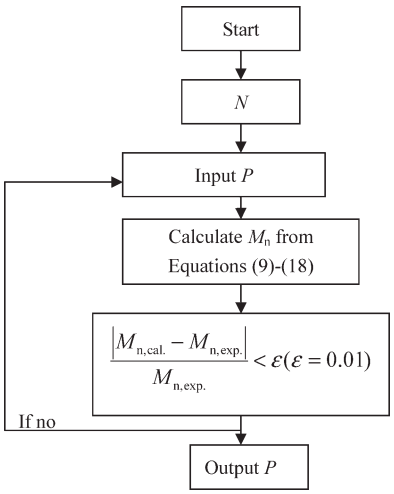

Figure 12. Flow chart of the calculation of *P*.

micromixing rate and the coalescence–redispersion frequency of the liquid elements with the increase of N.[25,59]

Calculation of P. The micromixing intensity of liquid–liquid on every cage in RPB can be characterized by the coalescence probability, which is defined as the percentage of droplet number participating in coalescence–redispersion process. The mixing intensity of liquid–liquid throughout the whole packing is denoted by the coalescence–redispersion frequency that is directly proportional to the coalescence probability at every cage. Therefore, a larger coalescence probability means a faster mixing rate, which is favorable for producing IIR with a higher M_n. Figure 12 illustrates the calculation process of P.

Figure 13 exhibits that ln P was linearly related to ln N. It was deduced,

$$P = 1.37 \times 10^{-6} \cdot N^{1.63}, \text{when } N < 1200 \text{ r min}^{-1} \qquad (19)$$

and $P = 0.15$, when $N \geq 1200$ r min^{-1} since M_n did not increase when N was more than 1200 r min^{-1}.

Model prediction: Effect of D

The above parameters were used to predict M_n vs. r*. Figure 14 shows the results of the simulated and experimental

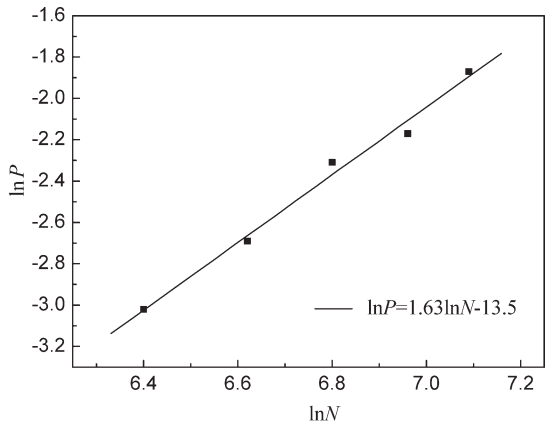

Figure 13. Effect of ln *N* on ln *P*.

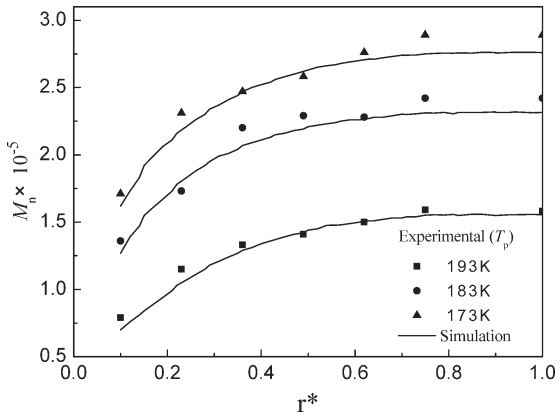

Figure 14. Experimental and simulated M_n vs. r* (N = 1200 r min^{-1}).

M_n with a changing D at different temperatures. It can be seen that M_n increased with the increase of D and then leveled off when D was more than 40 mm ($r^* = 0.75$). It was thus determined that the optimum packing thickness was 40 mm. It can also be seen from Figure 14 that the simulated M_ns fit well with the experimental M_ns, exhibiting the validity of the parameters in the model.

The results indicated that the inlet region of RPB plays a very important role in the mixing and reaction processes. The inlet region, also called end effect zone, refers to the part of the packing close to the inner edge of the rotator. It was revealed that strong micromixing occurs in the inlet region due to a large relative circumferential velocity and strong impingement between the liquid and the packing, resulting in a sharp increase of M_n in the inlet region. A slight increase of M_n in the bulk packing region (the part of the packing apart from the inlet region) was observed as a result of lower micromixing efficiency in this region compared to the inlet region.[25,49,59]

Model Validation

Figure 15 is the diagonal plot of all the simulation data and experimental values of M_n at different T_p, N, and D. It

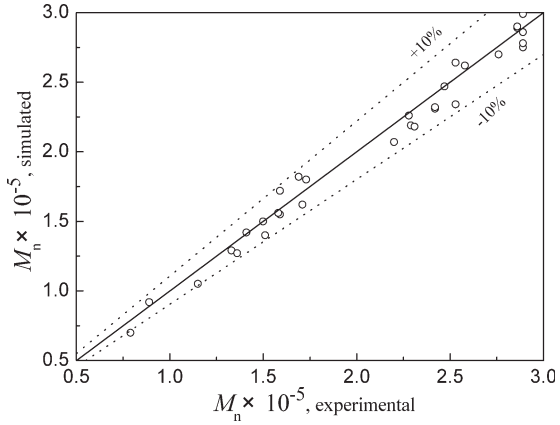

Figure 15. Diagonal graph of experimental and simulated M_n.

can be found that this model offers relatively precise predictions on the M_n of IIR prepared in RPB, with a deviation within 10% compared with the experimental values.

Conclusions

On recognition of conventional reactors' deficiency in micromixing for rapid cationic polymerization, rotaing packed bed was employed for the synthesis of IIR via cationic copolymerization of isobutylene and a small amount of isoprene. IIR with high production efficiency and high quality was obtained, which was attributed to the intensified micromixing performance of RPB. The optimum experimental conditions were determined at rotating speed of 1200 r min^{-1}, packing thickness of 40 mm and polymerization temperature of 173 K, where IIR with high molecular weight (M_n = 289,000) and unimodal molecular weight distribution (MWD = 1.99) was obtained. The mean residence time of the reaction process is less than 1 s in RPB while that is 30–60 min in conventional stirred tank reactors.[24] It is thus estimated that the production capacity per unit equipment volume is increased by 2–3 orders of magnitude, which reveals that RPB may be employed as a novel and efficient reactor for polymer synthesis by cationic polymerization in wide industrial applications.

A mathematical model to predict the M_n of IIR was developed. The model predicted M_n as a function of the polymerization temperature, rotating speed, and packing thickness. The results showed a good agreement between the simulated values and the experimental data. It is believed that this model could be used for cationic polymerization process development using RPB as a reactor.

Acknowledgments

This work was supported by NSFs of China (No. 20821004, No. 20990221 and No. 20774008) and the National "863" Program of China (No. 2006AA030202 and No. 2006AA030203).

Notation

$[A]$ = growing chain unit concentration, mol L^{-1}
$[C_1]$ = structural unit concentration, mol L^{-1}
$[C_2]$ = structural unit concentration, mol L^{-1}
D = packing thickness, mm
$[E_1]$ = end group concentration, mol L^{-1}
$[E_2]$ = end group concentration, mol L^{-1}
$[I]$ = initiator concentration, mol L^{-1}
$[I]_0$ = initial initiator concentration, mol L^{-1}
k_i = rate constant for initiation, L mol^{-1} s^{-1}
k_m = constant, 16
k_{p,M_1} = rate constant for propagation of M_1, L mol^{-1} s^{-1}
k_{p,M_2} = rate constant for propagation of M_2, L mol^{-1} s^{-1}
k_t = rate constant of termination, s^{-1}
$k_{tr,M1}$ = rate constant for chain transfer to M_1, L mol^{-1} s^{-1}
$[M_1]$ = isobutylene monomer concentration, mol L^{-1}
$[M_1]_0$ = initial isobutylene monomer concentration, mol L^{-1}
$[M_2]$ = isoprene monomer concentration, mol L^{-1}
$[M_2]_0$ = initial isoprene monomer concentration, mol L^{-1}
N = rotating speed, r min^{-1}
N_L = total cage number of packing, no
N_D = droplets number in every cage, no
P = coalescence probability
r^* = dimensionless form of r, $(r - r_i)/(r_o - r_i)$
r_i = inner radius of rotating packed bed, mm
r_o = outer radius of rotating packed bed, mm
t = time, s
$t_{1/2}$ = reactive characteristic time, ms
t_m = characteristic time of micromixing, ms
T_p = polymerization temperature, K

Greek letters

δ = distance between adjacent cages, mm
ε = energy dissipation rate per mass, w kg^{-1}
τ = mean residence time, s
υ = kinematic viscosities, m^2 s^{-1}

Literature Cited

1. Kennedy JP, Iván B. *Designed Polymers by Carbocationic Macromolecular Engineering: Theory and Practice*. Munich: Hanser, 1992.
2. Puskas JE, Kaszas G. Living carbocationic polymerization of resonance-stabilized monomers. *Prog Polym Sci*. 2000;25:403–452.
3. De P, Faust R. *Carbocationic polymerization*. In Matyjaszewski K, Gnanou Y, Leibler L, editors. *Macromolecular Engineering: Precise Synthesis, Materials Properties, Applications*. Weinheim: Wiley, 2007:57–101.
4. De P, Faust R. Carbocationic polymerization of isobutylene using methylaluminum bromide coinitiators: synthesis of bromoallyl functional polyisobutylene. *Macromolecules*. 2006;39:7527–7533.
5. Kostjuk SV, Dubovik AY, Vasilenko IV, Frolov AN, Kaputsky FN. Kinetic and mechanistic study of the quasiliving cationic polymerization of styrene with the 2-phenyl-2-propanol/ $AlCl_3{\cdot}OBu_2$ initiating system. *Eur Polym J*. 2007;43:968–979.
6. Li Y, Wu YX, Xu X, Liang LH, Wu GY. Electron-pair-donor reaction order in the cationic polymerization of isobutylene coinitiated by $AlCl_3$. *J Polym Sci Part A: Polym Chem*. 2007;45:3053–3061.
7. Held D, Iván B, Müller AHE. Kinetic treatment of slow initiation in living carbocationic polymerization and investigation of benzyl halides as initiators for the polymerization of isobutylene. *Macromolecules*. 1998;31:7199–7202.
8. Kostjuk SV, Radchenko AV, Ganachaud F. Controlled/living cationic polymerization of *p*-methoxystyrene in solution and aqueous dispersion using tris(pentafluorophenyl)borane as a lewis acid: acetonitrile does the job. *Macromolecules*. 2007;40:482–490.
9. Feng WL, Isayev AI. High-power ultrasonic treatment of butyl rubber gum: structure and properties. *J Polym Sci Part B: Polym Phys*. 2005;43:334–344.
10. Sawamoto M. Modern cationic vinyl polymerization. *Prog Polym Sci*. 1991;16:111–172.
11. Goethals EJ, Prez FD. Carbocationic polymerizations. *Prog Polym Sci*. 2007;32:220–246.
12. Kennedy JP, Macréchal E. *Carbocationic Polymerization*. New York: Wiley, 1982.
13. Schlaad H, Kwon Y, Sipos L, Faust R. Determination of propagation rate constants in carbocationic polymerization of olefins. 1. Isobutylene. *Macromolecules*. 2000;33:8225–8232.
14. Sipos L, De P, Faust R. Effect of temperature, solvent polarity, and nature of lewis acid on the rate constants in the carbocationic polymerization of isobutylene. *Macromolecules*. 2003;36:8282–8290.
15. Puskas JE, Chan SWP, Mcauley KB, Shaikh S, Kaszas G. Kinetics and mechanisms in carbocationic polymerization: the quest for true rate constants. *J Polym Sci Part A: Polym Chem*. 2005;43:5394–5413.
16. Sigwalt P, Moreau M. Carbocationic polymerization: mechanisms and kinetics of propagation reactions. *Prog Polym Sci*. 2006;31:44–120.
17. De P, Faust R. Living Carbocationic polymerization of *p*-methoxystyrene using *p*-methoxystyrene hydrochloride/$SnBr_4$ initiating system: determination of the absolute rate constant of propagation for ion pairs. *Macromolecules*. 2004;37:7930–7937.
18. De P, Sipos L, Faust R, Moreau M, Charleux B, Vairon JP. Determination of the propagation rate constant in the carbocationic polymerization of 2,4,6-trimethylstyrene. *Macromolecules*. 2005;38:41–46.
19. Matyjaszewski K, Pugh C. *Mechanistic aspects of cationic polymerization of alkenes*. In: Matyjaszewski K, editor. *Cationic Polymerization: Mechanisms, Synthesis, and Applications*. Dekker M Press: New York, 1996:192–204.

20. Qiu YX, Wu YX, Xu X, Ran F, Wu GY. Propagation rate constants for the cationic polymerization of vinyl monomer. *Chin Polym Bull*. 2006;4:1–10, 28.
21. Plesch PH. The propagation rate constants of the cationic polymerisation of alkenes. *Prog React Kinet*. 1993;18:1–62.
22. Puskas JE, Shaikh S, Yao KZ, McAuley KB, Kaszas G. Kinetic simulation of living carbocationic polymerizations. II. Simulation of living isobutylene polymerization using a mechanistic model. *Eur Polym J*. 2005;41:1–14.
23. Wu GY, Wu YX. *Controlling Cationic Polymerization and Its Application*. Beijing: Chemical Industry Press, 2005.
24. Liu DH. *Handbook of Synthetic Rubber Industry*. Beijing: Chemical Industry Press, 1991.
25. Yang HJ, Chu GW, Zhang JW, Shen ZG, Chen JF. Micromixing efficiency in a rotating packed bed: experiments and simulation. *Ind Eng Chem Res*. 2005;44:7730–7737.
26. Chen JF, Zheng C, Chen GT. Interaction of macro- and micromixing on particle size distribution in reactive precipitation. *Chem Eng Sci*. 1996;51:1957–1966.
27. Boodhoo KVK, Dunk WAE, Vicevic M, Jachuck RJ, Sage V, Macquarrie DJ, Clark JH. Classical cationic polymerization of styrene in a spinning disc reactor using silica-supported BF_3 catalyst. *J Appl Polym Sci*. 2006;101:8–19.
28. Kresge EN, Ver Strate GW. US Patent 4,666,619, 1987.
29. Kresge EN, Ver Strate GW. US Patent 4,575,574, 1986.
30. Marx RE, Nelson JM, Hanley KJ. US Patent 6,969,491 B1, 2005.
31. Chen GT. *Foundation of Polymer Reactive Engineering*. Beijing: China Petrochemical Press, 1991.
32. Li X, Chen JF, Chen GT. Morphological configurations of material elements during turbulent mixing-experimental study and modelling. *Acta Mech Sin*. 1994;26:266–271.
33. Chen JF, Wang YH, Guo F, Wang XM, Zheng C. Synthesis of nanoparticles with novel technology: high-gravity reactive precipitation. *Ind Eng Chem Res*. 2000;39:948–954.
34. Munjal S, Dudukovć MP, Ramachandran P. Mass transfer in rotating packed beds-I. development of gas-liquid and liquid-solid mass-transfer correlations. *Chem Eng Sci*. 1989;44:2245–2256.
35. Ramshaw C. Mallinson R. Mass transfer process. US Patent 4,263,255, 1981.
36. Chen JF, Shao L, Guo F, Wang XM. Synthesis of nano-fibers of aluminum hydroxide in novel rotating packed bed reactor. *Chem Eng Sci*. 2003;58:569–575.
37. Wang M, Zou HK, Shao L, Chen JF. Controlling factors and mechanism of preparing needlelike $CaCO_3$ under high-gravity environment. *Powder Technol*. 2004;142:166–174.
38. Chen JF, Shao L. Mass production of nanoparticles by high gravity reactive precipitation technology with low cost. *Chin Particuol*. 2003;1:64–69.
39. Guo K, Guo F, Feng YD, Chen JF, Zheng C, Gardner NC. Synchronous visual and RTD study on liquid flow in rotating packed-bed contactor. *Chem Eng Sci*. 2000;55:1699–1706.
40. Chen JF, Zhou MY, Shao L, Wang YH, Yun J, Chew NYK, Chan HK. Feasibility of preparing nanodrugs by high-gravity reactive precipitation. *Int J Pharm*. 2004;269:267–274.
41. Feng WL, Isayev AI. Continuous ultrasonic devulcanization of unfilled butyl rubber. *J Appl Polym Sci*. 2004;94:1316–1325.
42. Barsan F, Karam AR, Parent MA, Baird MC. Polymerization of isobutylene and the copolymerization of isobutylene and isoprene initiated by the metallocene derivative $Cp^*TiMe_2(\mu\text{-}Me)B(C_6F_5)_3$. *Macromolecules*. 1998;31:8439–8447.
43. Chung TC, Janvikul W, Bernard R, Hu R, Li CL, Liu SL, Jiang GL. Butyl rubber graft copolymers: synthesis and characterization. *Polymer*. 1995;36:3565–3574.
44. Feng WL, Isayev AI, von Meerwall E. Molecular mobility in ultrasonically treated butyl gum and devulcanized butyl rubber. *Polymer*. 2004;45:8459–8467.
45. Gronowski AA. Synthesis of butyl rubber in hexane using a mixture of Et_2AlCl and $EtAlCl_2$ in the initiating system. *J Appl Polym Sci*. 2003;87:2360–2364.
46. Zhang J. *An Experimental and Simulation Study on Liquid Flowing and Mass Transfer in RPB*. PhD Dissertation. Beijing, China: Beijing University of Chemical Technology, 1996.
47. Burns JR, Ramshaw C. Process intensification: visual study of liquid maldistribution in rotating packed beds. *Chem Eng Sci*. 1996;51:1347–1352.
48. Curl RL. Disperse phase mixing. 1. Theory and effects in simple reactors. *AIChE J*. 1963;9:175–181.
49. Guo K. *A Study of Liquid Flowing Inside the Higee Rotor*. PhD Dissertation. Beijing, China: Beijing University of Chemical Technology, 1996.
50. Shang LR, Wang JH. Modeling of poly(ethylene terephthalate) reactors and its application in the dynamic simulation of polymerization process. *Comput Simul*. 2003;20:2:99–102.
51. Shang LR. *Modeling of Poly(ethylene terephthalate) Reactors and Its Application in the Dynamic Simulation of Polymerization Process*. M. Dissertation. Beijing, China: Beijing University of Chemical Technology, 2000.
52. Wang JD. *Real-time dynamic simulation of low density polyethylene reactor under high pressure*. M. Dissertation. Beijing, China: Beijing University of Chemical Technology, 1997.
53. Pan ZR. *Polymer Chemistry*. Beijing: Chemical Industry Press, 2000.
54. Blavier L, Villermaux J. Free radical polymerization engineering-II: modeling of homogeneous polymerization of styrene in a batch reactor, influence of initiator. *Chem Eng Sci*. 1984;39:101–110.
55. Wang WS, Li SF. Conditional contractivity of Runge-Kutta methods for nonlinear differential equations with many variable delays. *Commun Nonlinear Sci Numer Simul*. 2009;14:399–408.
56. Thomas QA, Storey RF. Effect of reaction conditions on apparent $TiCl_4$ reaction order in quasiliving isobutylene polymerization at high [initiator]/[$TiCl_4$] ratios. *Macromolecules*. 2003;36:10120–10125.
57. Paulo C, Puskas JE, Angepat S. Effect of reaction conditions on the kinetics of living isobutylene polymerization at high initiator/$TiCl_4$ ratios. *Macromolecules*. 2000;33:4634–4638.
58. Fordor Z, Bae YC, Faust R. Temperature effects on the living cationic polymerization of isobutylene: determination of spontaneous chain-transfer constants in the presence of terminative chain transfer. *Macromolecules*. 1998;31:4439–4446.
59. Yang HJ, Chu GW, Xiang Y, Chen JF. Characterization of micromixing efficiency in rotating packed beds by chemical methods. *Chem Eng J*. 2006;121:147–152.

Manuscript received Jan. 25, 2008, and revision received Feb. 23, 2009.